IET Generation, Transmission & Distribution

Research Article

IET Journals
The Institution of Engineering and Technology

New intelligent controlled islanding scheme in large interconnected power systems

ISSN 1751-8687
Received on 4th May 2015
Revised on 22nd July 2015
Accepted on 12th August 2015
doi: 10.1049/iet-gtd.2015.0576
www.ietdl.org

Ghader Isazadeh, Amin Khodabakhshian ✉, Eskandar Gholipour

Electrical Engineering Department, University of Isfahan, Isfahan, Iran
✉ *E-mail: aminkh@eng.ui.ac.ir*

Abstract: This study presents a new intelligent controlled islanding scheme based on wide area measurement systems data to avoid the wide area blackout. Three offline, online and real-time parts are applied to solve three problems including where and when to implement islanding and what to do after separation. New security-based criteria are used to determine the initial stable coherent groups. The boundaries of islands are obtained adaptively considering different operating points by using the weighted time varying graph structure of the network. To reach more stable islands, reactive power is considered by using a self-tuned online fuzzy factor in graph weights. The number of necessary islands with their locations is determined in online part by monitoring the dominant inter-area oscillations between the initial groups (IGs). Then, the network is split into islands with the objective of minimum power flow disruption. To detect the unavoidable islanding cases correctly, a new parallel adaptive neuro-fuzzy inference system (ANFIS) structure is designed. In a parallel structure, for each of two adjacent IGs a distinct ANFIS is also applied to consider variable stability margins between groups. Simulation results confirm that the blackout can be avoided in a large power grid by using the proposed method.

1 Introduction

In recent years, the frequent occurrence of cascading outages at stressed conditions leads to have the uncontrolled network separation with unstable islands and, consequently major blackouts [1, 2]. To prevent such events in power system, controlled islanding, which is an automatic corrective action plan can be applied to split the network to self-healing islands [3].

In an effective islanding design, three main problems including where (proper locations), when (correct time) and what to do after islanding should be solved co-ordinately [3]. Two graph-based approaches including slow coherency (SC) [4] and ordered binary decision diagram [5] are widely used to solve the where problem. The objective of these approaches is to reach stable islands with minimum active power imbalance in each island considering generators coherency and static constraints. In [6], the concept of the minimum power flow disruption is used instead of minimal active power imbalance to prevent the power flow pattern from considerable changes. Furthermore, considering the only active power may lead to islands collapse due to reactive power shortage and voltage instability problems [7]. In [7], both active and reactive powers are considered in network partitioning, while generators coherency is ignored and this may lead to have unstable transient islands and as a result, the entire system will collapse.

In all of the above-mentioned methods, the fixed locations of islands are obtained based on the pre-known number of islands determined by offline stability studies [3–7]. Nevertheless, the number and locations of islands depend on the real-time system stability and generators coherency, which vary for different operating points and network topologies [8].

When the boundaries of islands are determined, the next concern is the execution time of islanding [4–7]. The late or unnecessary network splitting has disaster consequences in power system security. In many studies, the islanding execution is performed through the installation of the local out of step relays at specified lines. The reliability of these local relays is enhanced by using decision tree (DT) method based on recently developed wide area measurement systems (WAMS) [9]. In [10], the wide area information of network oscillations is used to detect unstable inter-area modes and to split the network to the fixed pre-determined locations. There are many different indices based on the mode shape, damping and phase angle of oscillations that are used to detect inter-area unstable swings [11, 12].

In this paper, a new intelligent controlled islanding scheme is designed based on wide area monitoring, protection and control (WAMPAC) system. The proposed response-based algorithm is divided into three offline, online and real-time parts to address the location and time of islanding and necessary corrective actions in islands. To expedite the algorithm for real-time application, the obtained initial coherent groups are replaced with the defined intermediate buses by using the assigned security-based criteria in offline part. The reactive power flows of lines are considered in the weights of the proposed time varying weighted graph of the network through a proposed online tuned factor. The number and the locations of the necessary islands are determined adaptively in online part by monitoring the dominant inter-area modes. At this part, a new multi-level constraint spectral clustering approach is utilised for network partitioning to reach stable islands with minimum power flow disruption. A new parallel adaptive neuro-fuzzy inference system (ANFIS) structure is also used to assess the real-time stability and to execute islanding. To account the variable stability margins between areas at different network conditions, the individual ANFIS is assigned to each of two adjacent initial groups (IGs). The fuzzy rules are derived by using the comprehensive stability studies and selecting proper wide area input signals. The proposed islanding method is applied to the IEEE 39-bus test system and Iran transmission network. The simulation results show that the accurate necessary islands with appropriate security levels are obtained online. Also, large-scale multi-area power systems such as Iran power grid become immune from wide area blackout at extreme unpredicted events. The capability of the ANFIS method to determine unnecessary islanding cases is also investigated.

2 Proposed islanding design

The flowchart of the proposed algorithm is shown in Fig. 1. Three main problems of the controlled islanding consisting of where,

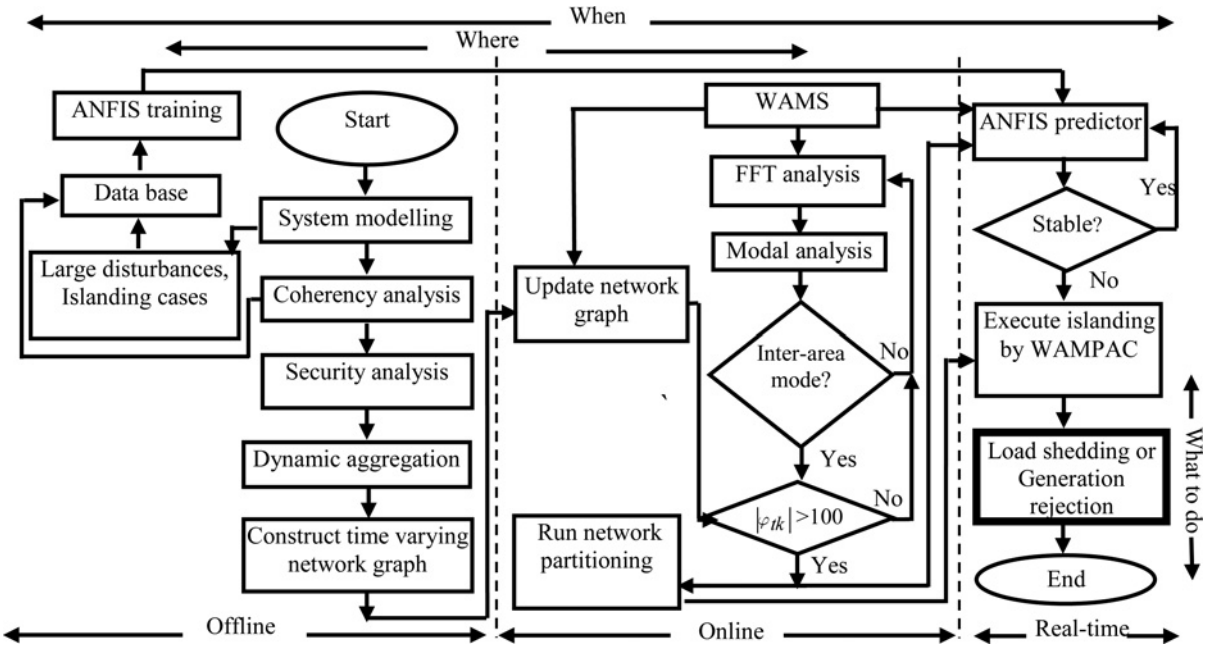

Fig. 1 *Flowchart of the proposed intelligent algorithm*

when and what to do are designed co-ordinately at three different parts of offline, online and real time. In the first problem (where), there are different steps in offline part including coherency and security analysis, dynamic aggregation and network graph construction. The number of islands and final boundaries are determined in online part for detecting dominant inter-area modes and their oscillation behaviours. To solve the when problem correctly, all of the three parts are involved. The final decision about islanding time execution is made in real-time part through the proposed parallel ANFIS structure. The database of the proposed ANFIS stability predictor is created through extensive offline stability studies. The problem of what to do after islanding is solved by applying load shedding, generation rejection and all necessary corrective actions.

3 Where to implement islanding

To determine the locations of islands, the following steps are applied.

3.1 Coherency analysis

At this step, the Fuzzy C-Medoids (FC-MDD) method given in [13] is used to determine the groups of buses that are always coherent together. In this method, the offline probabilistic coherency is applied at different loading conditions, load flow pattern and network topologies. In addition, unexpected extreme disturbances between interconnected areas that could lead to wide area instability are taken into account.

3.2 Dynamic network aggregation

To have the stable operation of islands after separation, the intermediate buses are determined to prevent the disconnection of some lines that lead to have islands with improper security margins. In this regard, the determined coherent generator buses with respect to the performed coherency analysis are aggregated to form IGs and are replaced with the intermediate buses. To determine these buses, the security criteria including available transfer path and loading of equipment in IGs, voltage magnitude of buses and relay margins of local distance relays [8] are applied to ensure that each IG could operate safely after separation even if there is a possibility to have next internal contingencies. The main advantage of this method is that IGs with positive stability margins are constructed. Besides, it ensures that the generators are coherent at each island and the network size is reduced to speed up the algorithm. To determine the optimal boundaries considering power flows and network structure in online part, the time varying graph structure of the network between determined IGs is created.

3.3 Time varying graph structure

The undirected weighted graph of the network $G(V, E, W)$ including lines (edges) between buses (nodes) is constructed [14]. V is a node set, E is an edge set and W is a set of edge weights. The graph edges (lines) between nodes (buses) are initially weighted ($w_{ij}(t)$) according to active power flow ($P(t)$), reactive power flow ($Q(t)$) and electrical line length (x) between each of two connected buses. As shown in (1), the final weights ($w'_{ij}(t)$) of edges are adjusted by α factor to change the role of the reactive power flow importance in the assigned combined weight. The graph structure and weights are updated in online part every 1 s to consider network changes.

$$\boldsymbol{P} = \begin{bmatrix} 1-\alpha \\ \alpha \end{bmatrix}, \quad w_{ij}(t) = \begin{bmatrix} \dfrac{P(t)}{x} & \dfrac{Q(t)}{x} \end{bmatrix}, \quad w'_{ij}(t) = \boldsymbol{P}^{\mathrm{T}} \cdot w_{ij}{}^{\mathrm{T}}(t) \tag{1}$$

3.4 Fuzzy factor α

The factor α in (1) is assumed to be a fuzzy variable, which is dependent on reactive power reserve and the voltage magnitudes of buses at each IG. Therefore, the inputs of the fuzzy set are as follows:

$$\Delta V = \sum_{i=1,k} (1 - V_i) \tag{2}$$

$$\Delta Q = \sum_{i=1,n} (Q_{i\max} - Q_{i\mathrm{gen}}) \tag{3}$$

where k and n are the buses and generators at each of determined IGs, respectively. In (2), V_i is the per unit value of voltage magnitude of the ith bus. Also, the $Q_{i\max}$ and $Q_{i\mathrm{gen}}$ in (3) are the maximum capability and actual reactive power values of the ith generator in per unit, respectively. These data are gathered from WAMS and

are updated every 1 s to adjust edge weights of graph in online part. The Gaussian membership function is applied to both of inputs and outputs [15]. There are three membership functions (big, small and zero) and five (negative big, negative small, zero, positive small and positive big) for ΔQ and ΔV inputs while the output has four (zero, small, medium and big) membership functions (see Table 7 in Appendix). The inputs are normalised to be in interval [−0.2, 0.2] for ΔV and [0, 1] for ΔQ, while the α value is normalised to be between 0 and 0.5. These intervals are used for two studied test systems given in Section 6.

3.5 Detection of inter-area oscillations

To measure the possibility of asynchronous oscillations between determined groups, this paper considers the difference of centre-of-inertia (COI) related to the rotor angle of generators between two groups, which is defined as follows:

$$\Delta\bar{\delta}_{\mathrm{COI}_{t,k}} = \left(\frac{1}{M_t}\sum_{i=1}^{N_t} M_i\delta_i - \frac{1}{M_k}\sum_{i=1}^{N_k} M_i\delta_i\right), \quad M_j = \sum_{i=1}^{N_j} M_i \tag{4}$$

where N_t and N_k are the number of units in two groups t and k, M_j is the total inertia of the jth group with respect to N_j generators. The phasor measurement units (PMUs) data about $\Delta\bar{\delta}_{\mathrm{COI}}$ are analysed at every time step (ΔT) over the last time window (T) in online part. The value of ΔT is considered to be 1 s. The T should be long enough to identify the inter-area modes that are normally in the range of 0.1–0.9 Hz [16]. Therefore, the T values between 30 and 60 s can be chosen, and is selected to be 60 s here to have accurate responses [16].

By applying modal analysis to the $\bar{\delta}_{\mathrm{COI}}$ between any two adjacent IGs, the squared-coherency function is computed by (5) to detect inter-area oscillations [16]

$$\gamma_{tk}^2(\omega) = \frac{|S_{tk}(\omega)|^2}{S_{tt}(\omega)\,S_{kk}(\omega)} \tag{5}$$

where $S_{tk}(\omega)$ is the cross-spectral density (CSD) of the related $\bar{\delta}_{\mathrm{COI}}$ between two groups t and k, and $S_{tt}(\omega)$ and $S_{kk}(\omega)$ are their power spectral densities, respectively. Any oscillation with the value of γ_{tk}^2 greater than 0.8 is considered as the inter-area mode. In the proposed algorithm, the top four sustained dominant inter-area modes (ω_n, $n = 1, \ldots, 4$) between each of adjacent IGs at every ΔT seconds are selected and monitored.

3.6 Islanding boundary

The phase angle (φ_{tk}) of S_{tk} higher than the threshold value of 100° at each determined inter-area frequency (f_n), is used as a sign of possible angle separation between two t and k adjacent IGs [16]. By simultaneously investigating the $\varphi(\omega_n)$ value for each of two adjacent IGs, the synchronous groups in ω_n with the number of necessary islands which could be one or a combination of adjacent IGs is derived. Then, as shown in Fig. 1, the graph partitioning algorithm is run to separate asynchronous IGs from each other in online part.

3.6.1 Objective function: The concept of the minimal power flow disruption is adopted as the objective function to avoid the disconnection of heavy loaded lines. It should be mentioned that using this objective function improves the transient stability of islands, reduces the probability of lines overloading and eases the islands reconnection to the entire network [6]. The objective function to partition the original graph G_0 (V_0, E_0, W_0) of the network into two islands V_1 and V_2 is as follows [14]:

$$\min_{V_1, V_{2\subset V}} \sum_{i\in V_1,\, j\in V_2} \left|w'_{ij}(t)\right| \tag{6}$$

$$\text{subject to } V_{\mathrm{G1}} \subset V_1,\ V_{\mathrm{G2}} \subset V_2,\ E_{\mathrm{s}} \neq 0 \text{ and } E_{\mathrm{s}} \subset E$$

where V_{G1} and V_{G2} are the subsets of determined coherent groups, while E_{s} is an edge set that should not be disconnected. With respect to the assigned criteria given in Section 3.2 in constructing secure IGs, static constraints including voltage magnitude of buses and loadings of lines are satisfied after separation. To partition the network into more than two islands, the recursive bisection method is used [14].

3.6.2 Multi-level graph partitioning: The constraint spectral clustering approach given in [6] is developed to the multi-level graph partitioning algorithm to have a fast and accurate response. Three phases of this algorithm are:

(i) *Coarsening phase:* During this phase, a sequence of smaller graphs (G_m (V_m, E_m, W_m)) is created from the original graph [17]. The heavy edge matching method is used to combine the edges with high weights and to reduce the graph size [17].

(ii) *Graph partitioning phase:* The normalised constrained spectral clustering approach is used to partition the reduced graph (G_m) into k islands [6]. The projection matrix is also utilised to ensure that the coherent groups are connected and asynchronous groups are disconnected from each other [6]. This projection matrix is updated in online part based on network oscillations to consider generators coherency and to solve the drawback of the spectral clustering approach for determining the number of necessary islands [6].

(iii) *Uncoarsening phase:* At this phase, the partition P_m *of* G_m (V_m, E_m, W_m) is projected back to the G_0 (V_0, E_0, W_0) by applying the KL algorithm [17].

4 When to implement islanding

As shown in Fig. 1, the procedure for determining the time of islanding is performed at three different offline, online and real-time parts. A comprehensive stability analysis at different loading conditions and network structures is performed offline to construct the database of the ANFIS stability predictor [18]. The modelling of local relays and network controllers based on their actual settings makes it possible determine the scenarios of large-scale cascading outages more accurately. To do this, different initial large disturbances including bus faults, faults in tie lines and outages of large generators are considered [19]. The fault clearing time is delayed intentionally to back-up relays operation in some scenarios to account the hidden failure of relays, which may include the loss of the whole substation and connected equipment. Then, in other scenarios, the relays margins are determined and equipment with lower margins is disconnected. To consider severe disturbances, the same procedure is applied for the multiple disturbances with fixed short time interval before the operation of corrective actions [20].

After asynchronous oscillations are detected in online part, the signal is sent to ANFIS predictor in the real-time part to make the final decision about the necessity and the execution time of islanding.

4.1 Real-time stability assessment

The ANFIS is used to derive the condition that the islanding execution is, or is not, a necessary task in real time.

4.1.1 ANFIS predictor: In practice, the stability margins between areas are different and vary with respect to the system operating point and network structure. It is shown in many cases that the loss of synchronism will be inevitable if the phase angle difference between areas becomes 120° [21]. For this reason, the parallel ANFIS structure, as shown in Fig. 2 is used with the individual ANFIS for each of two adjacent IGs. To consider the effect of different parameters in network stability, the proper wide area signals are employed as the ANFIS inputs. These signals are introduced in the following subsection.

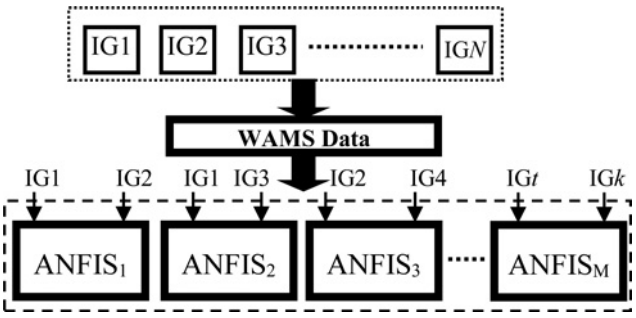

Fig. 2 *Proposed parallel ANFIS structure*

4.1.2 ANFIS structure: Many parameters may help to have a correct prediction of the system wide area instability and islanding cases. In addition to the signal given in (4), the following input signals are used as the input signals

$$\Delta\bar{\theta}_{t,k} = \left(\frac{1}{N}\sum_{i=1}^{N}\theta_i - \frac{1}{M}\sum_{j=1}^{M}\theta_j\right) \tag{7}$$

where $\Delta\bar{\theta}_{t,k}$ is the difference of average voltage angles between two groups t and k, and θ_i and θ_j are the voltage angles of buses at two groups t and k with N and M installed PMU. The difference of average frequency ($\Delta\bar{\omega}_{t,k}$) is defined as follows:

$$\Delta\bar{\omega}_{t,k} = \frac{\mathrm{d}\Delta\bar{\theta}_{t,k}}{\mathrm{d}t} \tag{8}$$

The difference between the average of voltage magnitudes of buses at two groups t and k is given as follows:

$$\Delta\bar{V}_{tk} = \left(\frac{1}{N}\sum_{i=1}^{N}V_i - \frac{1}{M}\sum_{j=1}^{M}V_j\right) \tag{9}$$

where V_i and V_j are the voltage magnitudes of N and M intermediate buses between two groups t and k with installed PMU. The sum of relay margin of distance relays between two groups of t and k is defined as follows

$$R \cdot M_{tk} = \sum_{i=1,l}\frac{Z_{\mathrm{act}_i}}{Z_{\mathrm{set}_i}} \tag{10}$$

where, Z_{act_i} and Z_{set_i} are the actual and setting values of the impedance at relays in line i between two groups of t and k. The Gaussian membership function is assigned for each of input variables [15]. The output of ANFIS for each two adjacent groups will be either 1 (unstable) or 0 (stable) to classify stable cases from unstable ones. The fuzzy rules are derived from time domain studies and are different for each of assigned ANFIS with respect to different stability margins between adjacent groups. Due to the limited space, the fuzzy rules for two IGs 8 and 9 in Iran power system are given, as an example in Table 8 in the Appendix. At the instant of identifying the unstable cases by ANFIS (output = Y = 1), the tripping signals are sent to the breakers of the determined lines through WAMPAC system.

5 What to do after islanding

After network separation, under frequency load shedding (UFLS), under voltage load shedding (UVLS) and generation rejection may be necessary to balance loads and generation in islands [4–7]. In the proposed islanding method, two-level UFLS, which can be easily adopted for power systems, is applied [22]. For the df/dt values greater than the determined threshold value (M), the static scheme is switched to adaptive, which is designed based on LD-df/dt method.

6 Simulation results

The IEEE 39-bus power system [6] and Iran power grid are chosen as test systems to apply the proposed controlled islanding method.

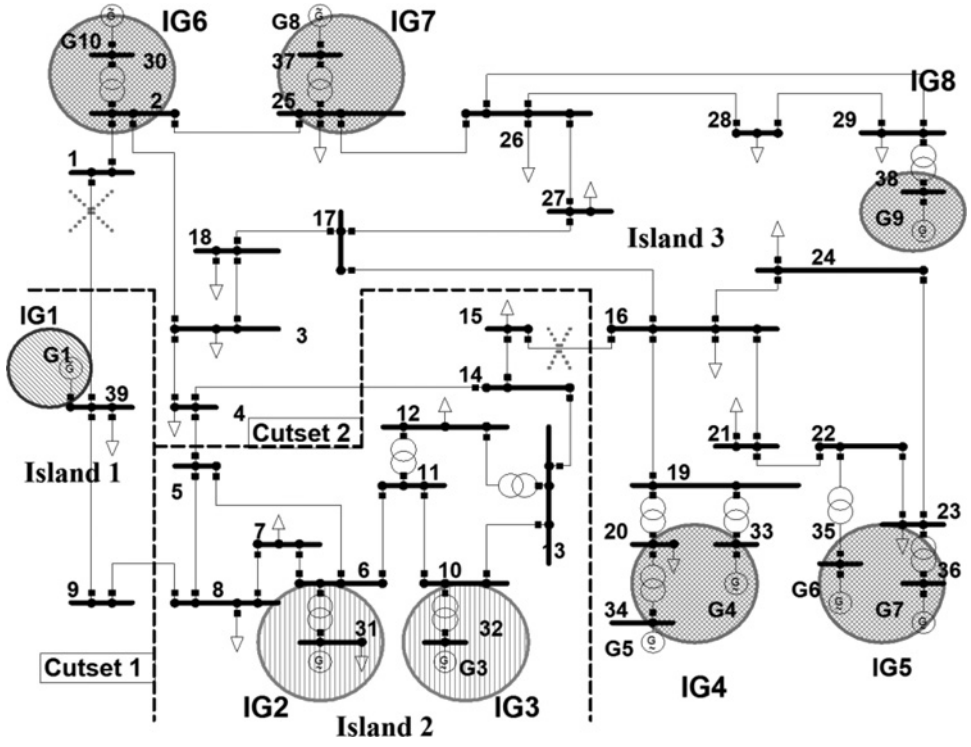

Fig. 3 *Determined IGs and islands boundaries in IEEE 39-bus power system for case 1*

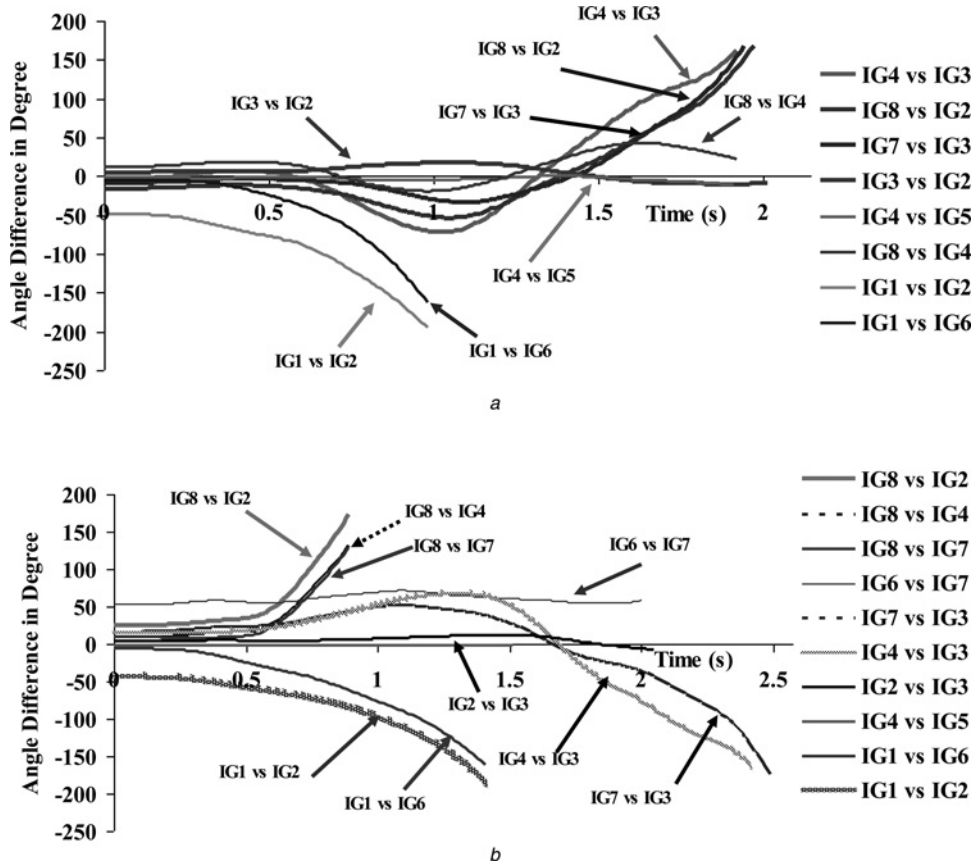

Fig. 4 *Angle separation between IGs in IEEE-39 bus for two test cases*

a Case 1
b Case 2

6.1. IEEE 39-bus power system

6.1.1 Islanding necessity and number of islands: The IGs of IEEE 39-bus power system are determined by applying the FC-MDD method and results are shown in Fig. 3. To investigate the performance of the designed islanding scheme, two different cases are considered. In case 1, the initial fault is applied at 0.1 s in lines 1–39 and the line is opened at 0.3 s by line breakers. Then, another fault is applied to lines 15 and 16 at 0.5 s and is cleared at 0.7 s by opening the faulted line. Monitoring the $\Delta\delta_{COI}$ values between adjacent IGs, as shown in Fig. 4*a* in online part, indicates that the network stability is lost and islanding execution is detected to be necessary by ANFIS structure. Investigation of angle separation between adjacent IGs reveals that the IG1 swings against two its adjacent IGs (IG2 and IG6). In addition, IG2 and IG3 swing together, while all of IG4–IG8 swing together separately and against IG2 and IG3. Therefore, it is found that the network should be split into three islands of IG1 (island 1), IG2 and IG3 (island 2), IG4–IG8 (island 3). The obtained cutsets 1 and 2 to partition the network to three necessary islands are depicted in Fig. 3.

The determined optimal cutsets are shown in Table 1 and compared with other two approaches given in [4, 6]. As can be seen in Table 1, the coherent groups determined by the proposed method for islands 2 and 3 are different with the results of [4, 6] because of using different approaches. In SC and two-step methods, the coherent groups are obtained offline for the specified operating condition and network structure. Therefore, changes in generators coherency and loadings of lines following different disturbances and subsequent outages could not be accounted. If a new fault or outage occurs during the operation of the system, these approaches are not able to determine the proper new islands. This drawback is overcome by the proposed method in online part, which is able to determine the new necessary islands based on the coherency of generators and loading changes as explained in Sections 3.5 and 3.6. This will be more highlighted for case 2.

In case 2, the initial and second faults are applied to lines 10–13 and 26–28, respectively, by the same time interval as the first case. As shown in Fig. 4*b*, IG8 which was synchronous with IG4–IG7 in case 1 in island 3, becomes asynchronous with them. In addition to IG1 as a distinct island, IG2 and IG3 swing together like case 1 and against all of IG4–IG7, which are coherent together. Therefore, according to Fig. 4*b*, the number of necessary islands is detected to be four by online part and their IGs are IG1 (island 1), IG8 (island 2), IG2–IG3 (island 3), IG4–IG7 (island 4), while the number of islands was three for case 1.

Table 1 Determined boundaries for the IEEE 39-bus at case 1

Method	Proposed method	SC method [4]	Two step method [6]
Island 1	(IG1)	(IG1)	(IG1)
Island 2	(IG2–IG3),	(IG2–IG5),	(IG2–IG5),
Island 3	(IG4–IG8)	(IG6–IG8)	(IG6–IG8)
Cutset 1	8–9,	1–39, 8–9,	1–2, 8–9,
Cutset 2	4–5, 4–14	3–18, 3–4, 17–27	3–18, 3–4, 17–27
computation time, s	0.002	several seconds	0.0032

6.1.2 Computation time: As shown in Table 1, the computation time, which is obtained by using a computer of Pentium 3 GHz with 8 G RAM, for the proposed method in network partitioning phase to form three islands is only 2 ms and is lower than other two methods. This confirms that the proposed method is suitable for online applications.

In the next subsection by using the Iran power grid as another test system, more discussions will be given to show the advantages of the proposed method, especially when the designed parallel ANFIS structure is used.

IET Gener. Transm. Distrib., 2015, Vol. 9, Iss. 16, pp. 2686–2696

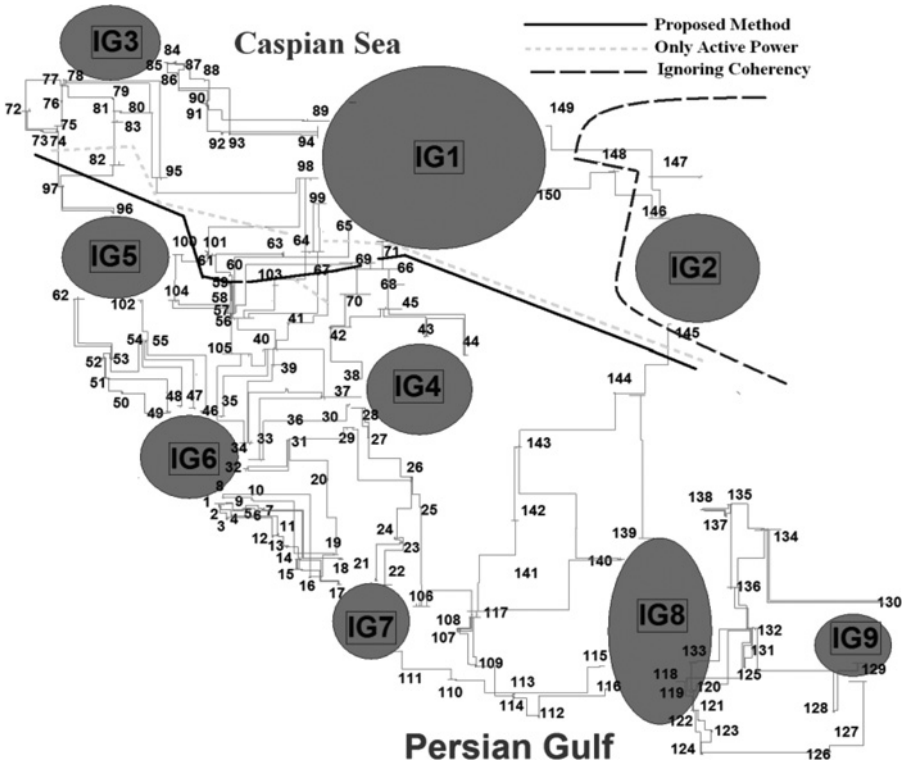

Fig. 5 *Islands boundaries for splitting the network to two stable islands*

6.2. Iran power network

The Iran power grid, as shown in Fig. 5, is a multi-area interconnected 400 and 230 kV networks in a wide spread geographical areas. The total installed generation capacity in year of 2014 is 65,000 MW. Three different loading conditions are shown in Table 2 [23]. The Iran power network had two major blackouts in years of 2001, 2002, and many considerable blackouts in recent years. There are many problems in this network such as overloading, voltage decline and unstable power swings at different contingencies [23]. Investigating the recent blackouts shows that the hidden failure of protection equipment and the wrong operation of local relays at stressed conditions make system so vulnerable to cascading failures. Therefore, in this study, all of effective local relays such as distance and over current relays, frequency and voltage protection of buses and generator excitation protection are considered. Now the islanding procedure given in Fig. 1 is applied to the Iran power grid and will be described in the following subsections.

6.2.1 Coherency analysis: By using the FC-MDD method, it is found that there are nine permanent coherent groups in the Iran power network. The graph structure of the system after aggregation is shown in Fig. 5. The generators in the west part of the network have the variable coherency behaviour. These fuzzy generators are assigned as the independent initial coherent group.

6.2.2 Network islanding: To investigate the performance of the proposed method in islands boundary determination, two different loading conditions as case 1 (summer) and case 2 (autumn) are considered (see Table 2). It is found that following a large disturbance in the centre part of power grid, IG1–IG3 swings against IG4–IG9 in both cases and two islands should be formed. Fig. 5 depicts the boundary lines of islands for case 1 when two methods of A (both active and reactive power flows) and B [only active power flow when $\alpha = 0$ as given in (1)] are taken into account.

Following determining these boundary lines, the extracted results are summarised in Table 3. In this table, the obtained results for SC method (method C) are also shown for comparison. It can be seen from Table 3 that the total active and reactive power flows of the disconnected lines for both cases are much lower in methods A

Table 2 Three loading conditions in the Iran power network [23]

Season	Loading condition	Total system load, MW
winter	light	31,600
autumn and spring	medium	42,750
summer	peak	58,000

Table 3 Determined boundaries for three investigated methods

Method	Both active and reactive powers (Method A)		Only active power (Method B)		SC method (Method C)	
Operating point	Case 1	Case 2	Case 1	Case 2	Case 1	Case 2
number of tripped lines	10	9	9	9	11	10
total active power of cutset (MW)	1563	1689	1354	1517	2357	2572
total reactive power of cutset (MVAr)	435	650	790	885	1029	1374
active power imbalance (MW) in island 1	−3578	−3699	−3475	−3580	−3254	−3313
reactive power imbalance (MVAr) in island 1	−25	−254	−188	−422	−654	−740
active power imbalance (MW) in island 2	+3633	+3745	+3523	+3631	+3341	+3388
reactive power imbalance (MVAr) in island 2	+650	+725	+890	+1120	+890	+1050
load shedding (MW) in island 1	3024	3165	2965	3034	2896	2992
generation shedding (MW) in island 2	2987	3076	2987	2995	2911	2987

Table 4 Computation time of proposed algorithm

Part		Time, s
	offline	several minutes depending on network size
online	detection of inter-area modes	0.85
	network graph partitioning	0.13
	real time	instantaneous

Table 5 Effect of α variation for case 2

α factor	Number of tripped lines	Total active power, MW	Total reactive power, MVar	Active power imbalance in island 1, MW	Active power Imbalance in island 2, MW
0	9	1689	650	−3699	+3745
0.1	9	1689	650	−3699	+3745
0.15	10	1890	470	−3934	+3975
0.25	9	2112	325	−4158	+4214
0.35	9	2112	325	−4158	+4214
0.5	11	2454	234	−4461	+4509

and B than method C because of their assigned objective function to have minimum power flow disruption [see (6)]. This difference is more evident for the reactive power flow. However, the active power imbalances in islands for method C are less than two other methods due to its objective function to have islands with minimum power imbalance. It should be noted that to reach this objective the number of disconnected lines is larger in method C.

In addition, it is clear from Table 3 that for case 1, as an example, the difference between the active power imbalance obtained for methods A and C is 324 MW, while the difference between their load shedding amounts is much less (128 MW). The reason for this outcome is that the reactive power imbalance in method C is much larger and UVLS has to be used to keep the voltage stability [24]. Nevertheless, this is not a necessary action for the proposed method since the reactive power is considered in the combined weight of the network graph [see (1)]. It should be noted that the difference between the active power imbalance and load shedding amount for all methods has been compensated by increasing the output of generators by the action of governors.

Therefore, by applying method A not only a desirable stability margin has been achieved because of preventing the heavy-loaded lines from disconnection, but also a more security margin is obtained by minimising the reactive power imbalance. As shown in Table 3, the disconnected lines are different for both cases in method A. This indicates that the proposed time varying graph structure of the network considers the loading changes of lines in different seasons.

It can be also seen from Fig. 5 that ignoring the coherency of generators leads to separate IG2 from the rest of network to form two islands, which is far away from feasible solutions and results in unstable islands. The computation time of the algorithm in different parts are given in Table 4, which indicates the advantage of the proposed method.

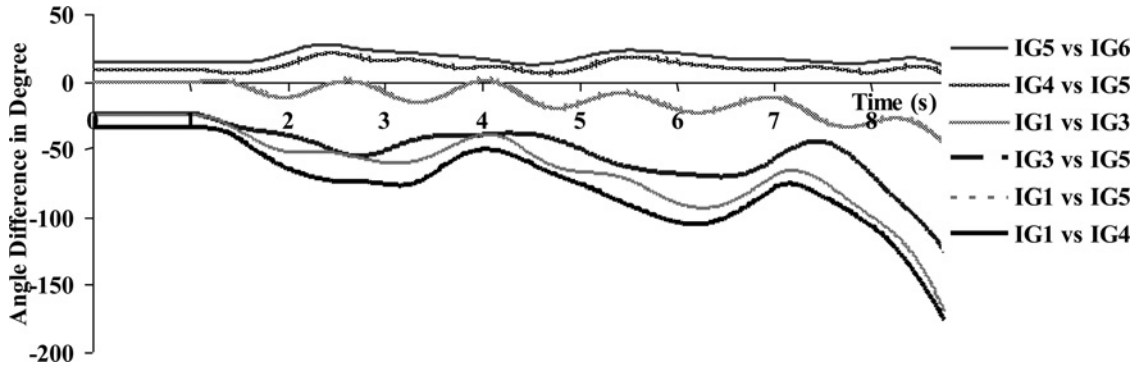

Fig. 6 *Angle separation to two islands in degree at scenario A*

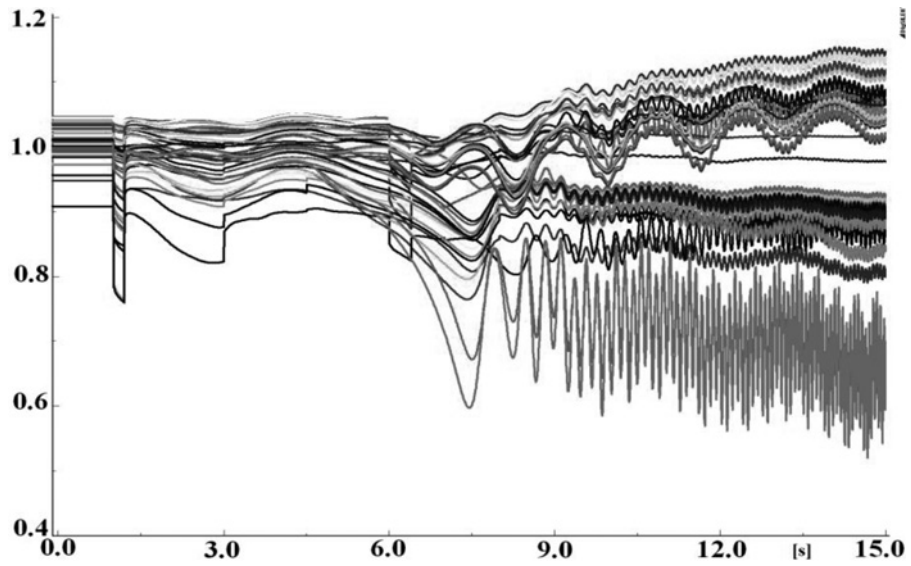

Fig. 7 *Voltage instability of network in southern areas in scenario B*

IET Gener. Transm. Distrib., 2015, Vol. 9, Iss. 16, pp. 2686–2696

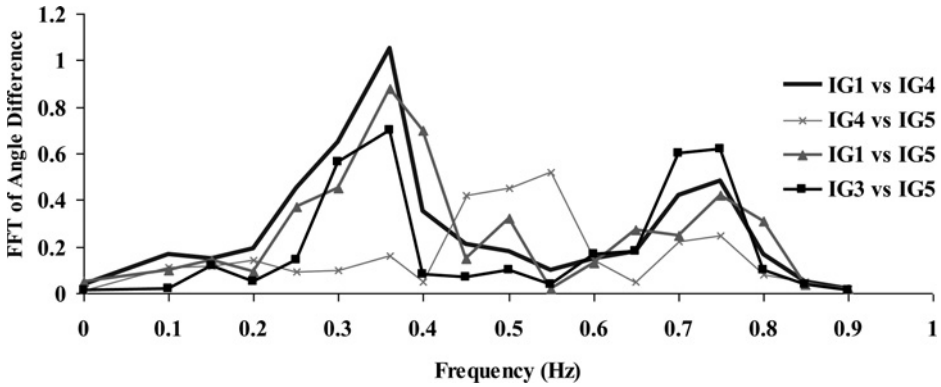

Fig. 8 *FFT on angle difference between some involved groups in 0.36 Hz*

Moreover, the effect of factor α [see (1)] in the sum of active and reactive power flows of the cutset and active power imbalance in islands is shown in Table 5. It can be seen that by increasing α, the sum of reactive power flow of the cutset is decreased, while the active power imbalance in islands increases. This shows that the α factor should be chosen properly to avoid unnecessary active power imbalance in islands.

6.2.3 Blackout scenarios in the Iran power grid: In the followings, two different scenarios that lead to wide area instability, uncontrolled separation and finally major blackout in the Iran power grid are given. The DSA tools [25] and DigSILENT power factory software [26] are used to perform the security analysis and time domain simulations. The overall events of these scenarios are as follows:

Scenario A: In the spring loading condition (see Table 2), a 600 MW generator unit is tripped due to the boiler failure in IG1. The loadings of interconnected lines to IG1 from adjacent IGs became higher. At this condition, a three-phase fault occurs near to bus 56. The circuit breaker failure leads to the disconnection of all 230 and 400 kV tie lines connected to this substation including some lines to IG1. The remained parallel lines connected to IG1 from IG4 to IG6 are overloaded, and unstable power swings appear between north-centre and south-centre areas. The operation of local relays makes some of remained lines and 800 MW generation units in northern area be disconnected. As a result, the network is separated to two unstable islands, as shown in Fig. 6, and are collapsed very fast due to the lines overloading, operation of local relays and under frequency condition.

Scenario B: In the summer loading condition, a single phase short circuit occurs in one of the two interconnected 400 kV lines

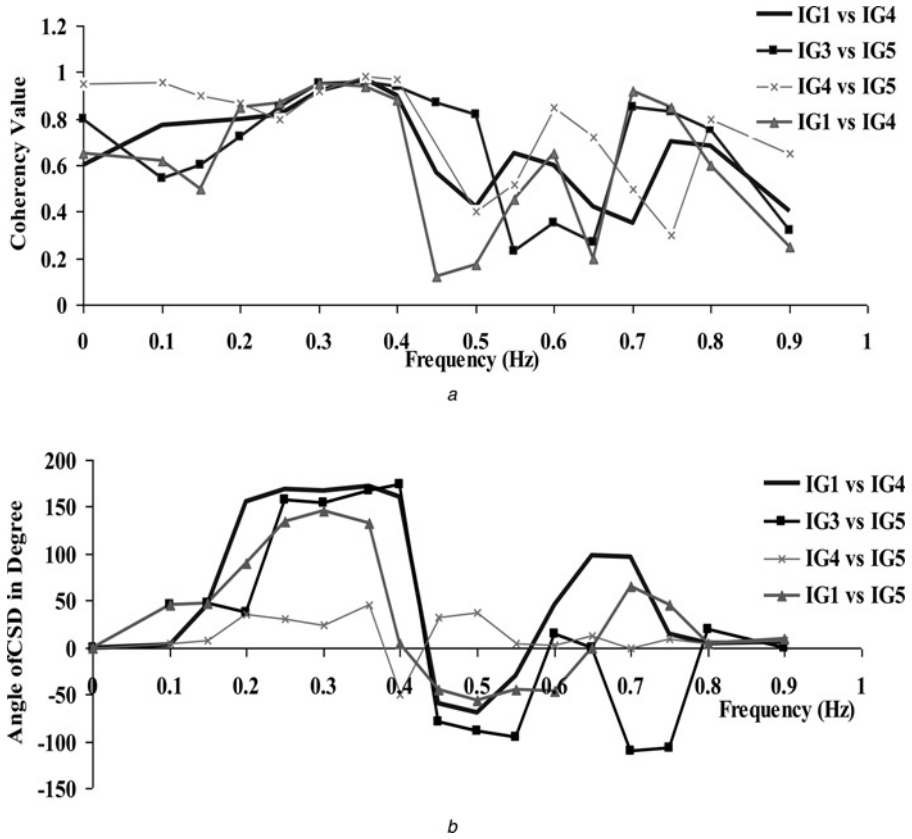

Fig. 9 *Mode shape analysis*

a Coherency value
b CSD angle

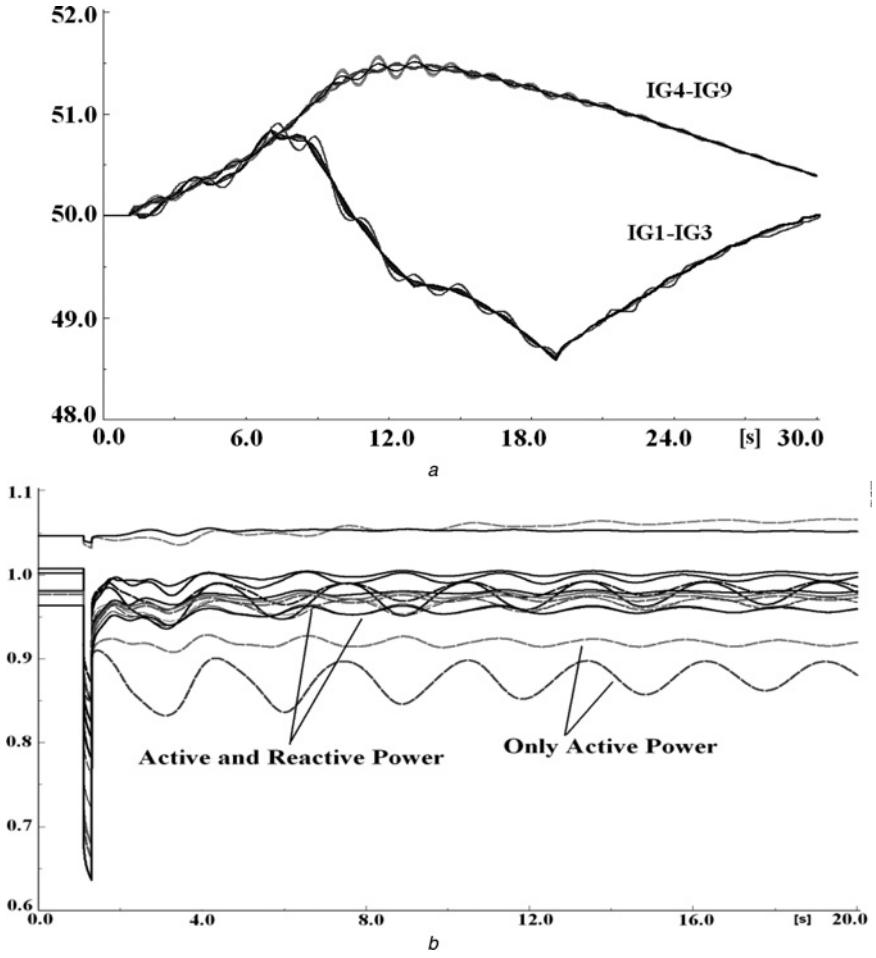

Fig. 10 *Islands parameters after network splitting*

a Frequency in Hz
b Voltage in p.u

between southern regions and both are then tripped. This event causes to have the loading increase and a voltage decline in many parts of southern areas. At this condition, losing 1000 MW generation in south due to the excitation protection makes the rest of 400 and 230 kV lines be tripped because of overloading and voltage decline. Consequently, as shown in Fig. 7, the interconnected lines are tripped by local relays and the southern part of the network becomes unstable and collapsed with 42% of network load.

7 Controlled islanding application

The proposed controlled islanding design is now applied to the blackout scenarios given in Section 6.2.3.

7.1 Scenario A

The results of fast Fourier transform (FFT) analysis of $\Delta\bar{\delta}_{COI}$ between some involved groups are shown in Fig. 8. It can be seen that the two dominant frequencies between these groups are 0.36 and 0.75 Hz. The coherency values between selected IGs are shown in Fig. 9*a*, which indicate that these two frequencies are inter-area modes. The CSD angles (φ_{tk}) of $\bar{\delta}_{COI}$ at these frequencies are then calculated to detect possible asynchronous oscillations and the results are shown in Fig. 9*b*. As can be seen from this figure, IG1 and IG3 swing against IG4 and IG5 at only the frequency of 0.36 Hz. By analysing the φ_{tk} value of the $\bar{\delta}_{COI}$ between each of adjacent IGs, it is found that the IG1–IG3 swing against all of IG4–IG9 at the frequency of 0.36 Hz. Therefore, the command signal is sent to the online part to determine the boundaries to separate the network into two islands. By receiving real-time data continuously, the islanding necessity is detected by using parallel ANFIS structure just one second after the final event happens. The output of the assigned ANFIS between each of IG1, IG2 and IG3 to their adjacent IGs (see Fig. 5) becomes near to unity (>0.9988) which indicates that there are asynchronous oscillations between these three groups to other groups. However, the ANFIS outputs between adjacent groups like IG1–IG2 and IG1–IG3 are close to zero (<0.002). This shows that there are synchronous oscillations between these three groups. Fig. 10*a* shows the frequency of two islands after islanding which clearly demonstrates the accurate actions of the proposed algorithm to keep the islands integrity and stability. The voltage stability of buses in islands, as shown in Fig. 10*b*, is much better than the condition when only active power is considered. As can be seen from Table 6, the magnitudes of voltages of buses are in the acceptable ranges and this accordingly avoids of operating the under voltage protection of buses and further outages.

As explained before, one of the main advantages of the proposed algorithm is that it will carry out controlled islanding if it is necessary. Therefore, to show this important capability of the algorithm scenario C is given in the following subsection.

7.2 Scenario C

It is assumed that instead of tripping two 400 kV lines that resulted in cascading outages and blackout in scenario B, only one of them is tripped due to a short circuit. In this case, it is found that the islanding execution is not necessary and system will be stabilised properly with one step UFLS at entire network and one step UVLS in IG9. This is shown in Fig. 11 in which the frequency

IET Gener. Transm. Distrib., 2015, Vol. 9, Iss. 16, pp. 2686–2696

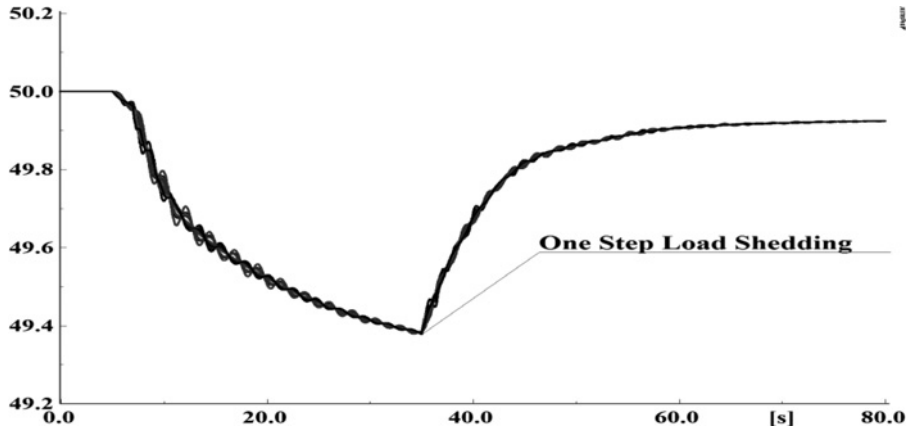

Fig. 11 *Frequency of network buses in Hz after one step load shedding*

Table 6 Voltage magnitude criteria at islands for two different methods

Scenario	A		B	
Method	Active	Active and reactive	Active	Active and reactive
min. voltage, p.u.	0.87	0.935	0.865	0.93
ave. voltage, p.u.	0.926	0.974	0.924	0.965
max. voltage, p.u.	1.072	1.051	1.065	1.053

variation of the system has been given. The ANFIS output between IG4–IG7 and IG6–IG7 that was near to unity in the blackout scenario B, becomes 0.0035 in this scenario. This indicates that the system is stable and there is no need for the execution of islanding. The main reason for this result is that the frequency drop in the whole network is almost identical. Also, there is one additional high capacity 400 kV interconnected tie line between IG6 and IG7 which prevents the 230 kV tie lines from being overloaded.

8 Conclusion

A new intelligent controlled islanding design is presented in this paper. To have a fast and accurate response base algorithm, the extensive offline studies are performed to aggregate initial network by considering generators coherency and security based criteria. The determination of islands boundary is addressed by considering a time varying graph structure. The effect of the reactive power is taken into account in the assigned combined weights of network graph that are updated online. At the instant of detecting the possible asynchronous oscillations in online part, the final boundaries are updated to consider loading and network structure changes. The time of the islanding execution is determined by using parallel ANFIS structure to detect unavoidable islanding cases in real-time based on WAMS data. Finally, the adaptive UFLS are implemented in network to keep islands integrity after network separation. The designed method has been applied to IEEE 39-bus and Iran power networks at the extreme contingency events. It is shown that with the proposed method, in addition to avoiding the wide area blackout, more stable islands with proper security levels have been reached.

9 References

1 NERC: 'Technical analysis of the August 14, 2003, blackout: what happened, why, and what did we learn?' (NERC, 2004), pp. 1–124

2 UCTE: 'Final report system disturbance on 4 November 2006' (UCTE, 2007), pp. 1–85

3 You, H., Vittal, V., Wang, X.: 'Slow coherency-based islanding', *IEEE Trans. Power Syst.*, 2004, **19**, (1), pp. 483–491

4 Xu, G., Vittal, V.: 'Slow coherency based cutset determination algorithm for large power systems', *IEEE Trans. Power Syst.*, 2010, **25**, (2), pp. 877–884

5 Sun, K., Zheng, D., Lu, Q.: 'Searching for feasible splitting strategies of controlled system islanding', *IEE Proc., Gener. Transm. Distrib.*, 2006, **153**, (1), pp. 89–98

6 Ding, L., Gonzalez, F., Wall, P., *et al.*: 'Two-step spectral clustering controlled islanding algorithm', *IEEE Trans. Power Syst.*, 2013, **28**, (1), pp. 75–84

7 Li, J., Liu, C., Schneider, K.: 'Controlled partitioning of a power network considering real and reactive power balance', *IEEE Trans. Smart Grid*, 2010, **1**, (3), pp. 261–269

8 EPRI: 'Power system transmission protection: challenges and research needs' (EPRI, 2004), pp. 1–66

9 Senroy, N., Heydt, G., Vittal, V.: 'Decision tree assisted controlled islanding', *IEEE Trans. Power Syst.*, 2006, **21**, (4), pp. 49–59

10 Sun, K., Hur, K., Zhang, P.: 'A new unified scheme for controlled power system separation using synchronized phasor measurements', *IEEE Trans. Power Syst.*, 2011, **26**, (3), pp. 1544–1554

11 Cepeda, J., Rueda, J., Colomé, D., *et al.*: 'Real-time transient stability assessment based on centre-of-inertia estimation from phasor measurement unit records', *IET Gener. Transm. Distrib.*, 2014, **8**, (8), pp. 1363–1376

12 Franco, R., Sena, C., Taranto, G., *et al.*: 'Using synchrophasors for controlled islanding – a prospective application for the Uruguayan power system', *IEEE Trans. Power Syst.*, 2013, **28**, (2), pp. 2016–2024

13 Kamwa, I., Pradhan, A., Joos, G., *et al.*: 'Fuzzy partitioning of a real power system for dynamic vulnerability assessment', *IEEE Trans. Power Syst.*, 2009, **24**, (3), pp. 1356–1365

14 Ding, L., Wall, P., Terzija, V.: 'Constrained spectral clustering based controlled islanding', *Int. J. Electr. Power Energy Syst.*, 2014, **63**, pp. 687–694

15 Jang, J.S.R., Sun, C.T.: 'Neuro-fuzzy modeling and control', *Proc. IEEE*, 1995, **83**, (3), pp. 378–406

16 Trudnowski, D.J.: 'Estimating electromechanical mode shape from synchrophasor measurements', *IEEE Trans. Power Syst.*, 2008, **23**, (3), pp. 1188–1195

17 Li, F., Zhang, Q., Zhang, W.: 'Graph partitioning strategy for the topology design of industrial network', *IET Commun.*, 2007, **1**, (6), pp. 1104–1110

18 Kamwa, I., Samantaray, S.R., Joos, G.: 'Development of rule-based classifiers for rapid stability assessment of wide-area post-disturbance records', *IEEE Trans. Power Syst.*, 2009, **24**, (1), pp. 258–270

19 EPRI: 'Detection, prevention and mitigation of cascading events' (EPRI, 2008), pp. 1–164

20 Vaiman, M., Bell, K., Chen, Y., *et al.*: 'Risk assessment of cascading outages: methodologies and challenges', *IEEE Trans. Power Syst.*, 2012, **27**, (2), pp. 631–641

21 Mei, K., Rovnyak, S.M.: 'Response-based decision trees to trigger one-shot stabilizing control', *IEEE Trans. Power Syst.*, 2004, **19**, (1), pp. 531–537

22 Seyedi, H., Sanaye-Pasand, M.: 'New centralised adaptive load-shedding algorithms to mitigate power system blackouts', *IET Gener. Transm. Distrib.*, 2009, **3**, (1), pp. 99–114

23 E.R.E.C: 'Security analysis in Iran power network; problems and solutions' (E.R.E.C, 2014), pp. 1–234

24 Otomega, B., Glavic, M., Van Cutsem, T.: 'Distributed under voltage load shedding', *IEEE Trans. Power Syst.*, 2007, **22**, (4), pp. 2283–2284

25 'DSA Tools'. Software available at: http://www.dsatools.com

26 'DigSILENT Power Factory'. Software available at: http://www.digsilent.de/

10 Appendix

See Tables 7 and 8.

Table 7 Fuzzy rules for α factor

	ΔV				
ΔQ	NB	NS	Z	PS	PB
B	Z	Z	Z	S	S
S	Z	S	S	M	M
Z	S	M	M	B	B

B: big, S: small, M: medium, Z: zero, NB: negative big, NS: negative small, PS: positive small, PB: positive big.

Table 8 Some of fuzzy rules for ANFIS between IG8 and IG9 in the Iran power grid

$\Delta\tilde{\theta}_{tk}$	$\Delta\tilde{\omega}_{tk}$	$\Delta\tilde{V}_{tk}$	$R.M_{t,k}$	Y	$\Delta\tilde{\theta}_{tk}$	$\Delta\tilde{\omega}_{tk}$	$\Delta\tilde{V}_{tk}$	$R.M_{t,k}$	Y
PB	PB	PM	PS	1	NB	NM	PM	PS	1
PB	PM	NM	Z	1	PM	PB	PB	PS	1
PB	PM	PM	Z	1	PS	PB	PS	PS	0
PM	PM	PB	PS	1	PM	PS	PS	PB	0
NB	NB	NM	Z	1	PB	Z	PM	PS	0
PB	PM	PB	Z	1	PS	PS	NS	PB	0
PS	PS	PM	PM	0	PS	PS	NS	PM	0

PB: positive big, PM: positive medium, Z: zero, PS: positive small, NB: negative big, NM: negative medium, NS: negative small.